ACS Photonics

pubs.acs.org/journal/apchd5

Article

Sequential Three-Dimensional Nonlinear Photonic Structures for Efficient and Switchable Nonlinear Beam Shaping

Chaowei Wang,[⊥] Pengcheng Chen,[⊥] Dunzhao Wei,[⊥] Leran Zhang, Zihang Zhang, Liqun Xu, Yanlei Hu, Jiawen Li, Yong Zhang,* Min Xiao, Jiaru Chu, and Dong Wu*

Cite This: *ACS Photonics* 2023, 10, 456−463

Read Online

ACCESS | Metrics & More | Article Recommendations | Supporting Information

ABSTRACT: Nonlinear beam shaping can be dynamically controlled by temperature or polarization to form switchable nonlinear structured beams, which constitute an unprecedented system for realizing optical encryption at new frequencies and high-dimensional nonclassical light sources. However, previous works were limited by a trade-off between the conversion efficiency and the modulation dimension of the beam. It is still technologically challenging to achieve efficient and switchable multidimensional nonlinear beam shaping. Here, we demonstrate switchable generation of nonlinear structured beams *via* three-dimensional (3D) nonlinear photonic crystals (NPCs) fabricated by femtosecond laser writing technique with considerable conversion efficiency. The 3D NPCs contain different sequential 3D arrays of spatially modulated $\chi^{(2)}$ nonlinearity designed by computer-generated hologram (CGH) along the optical *y*-axis ($LiNbO_3$ crystal). The output direction of the nonlinear beams can be changed by the carrier frequencies, while their efficiencies can be increased by the quasi-phase matching condition.

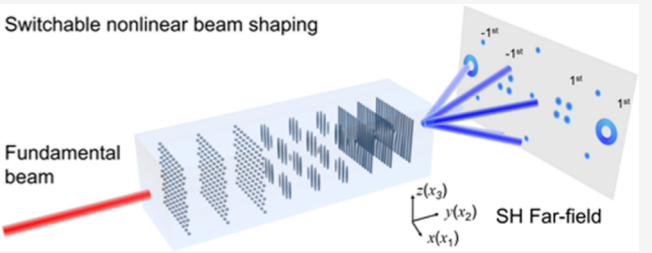

KEYWORDS: *femtosecond laser writing, switchable nonlinear beam shaping, quasi-phase-matching, wavelength-multiplexed technique*

INTRODUCTION

Optical beam shaping refers to the manipulation of a light source in terms of its fundamental properties including intensity, phase, and polarization, to produce a custom structured beam.[1−4] Switchable generation of structured beams further enriches their applications in various cutting-edge areas. Popular switching technologies are based on linear optical elements such as liquid crystals (LCs),[5,6] metasurfaces,[7,8] and photonic crystals.[9,10] Moreover, transferring the switching technologies developed from linear optical wavefront engineering to the nonlinear regime will open a new avenue for the realization of compact and ultrafast optical devices.

Nonlinear photonic crystals[11−14] and nonlinear metasurfaces[15−20] have been demonstrated to be important toolkits for nonlinear beam shaping. These nonlinear structures are constructed by artificially engineering the spatial distribution of nonlinear coefficients, which provides regular or irregular multiple reciprocal vectors to shape nonlinear waves in the far field through quasi-phase matching (QPM),[21,22] nonlinear Raman−Nath diffraction,[23] nonlinear Cerenkov radiation,[24] nonlinear Bragg refraction,[25] and so on. In particular, the QPM scheme largely increased the nonlinear conversion efficiency for shaping nonlinear quantum sources.[26] In the past decade, significant progress on switchable beam shaping using the nonlinear optical microstructures mentioned above has been reported. Nonlinear metasurfaces have advantages in the continuous modification of intensities or phases for switchable beam shaping.[27−30] However, the limited nonlinear interaction length resulted in low conversion efficiency. Switchable shaping of nonlinear structured beams can also be achieved using NPCs.[31−34] Nonlinear beams shaping in free space require two dimensions for full wavefront modulations while QPM requires another dimension to enhance conversion efficiency. Therefore, 2D NPC for nonlinear wave control has a trade-off between the conversion efficiency and the modulation dimension of beam (Figure S1, Supporting information). For example, the general configuration in previous works is based on nonlinear Raman−Nath diffraction, in which the phase matching condition is partially satisfied (i.e., there exists a certain phase mismatch). It can realize a two-dimensional beam, but the conversion efficiency is low. Although the 2D NPC could achieve more efficient SHG due to millimeter interaction length, it can only modulate one dimension in the transverse plane (i.e., Airy beam). Recently, 3D NPCs have been implemented by the femtosecond laser writing technique.[35−38] The increasing channel provides more abundant reciprocal vectors to efficiently modulate the

Received: October 3, 2022
Published: January 20, 2023

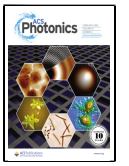

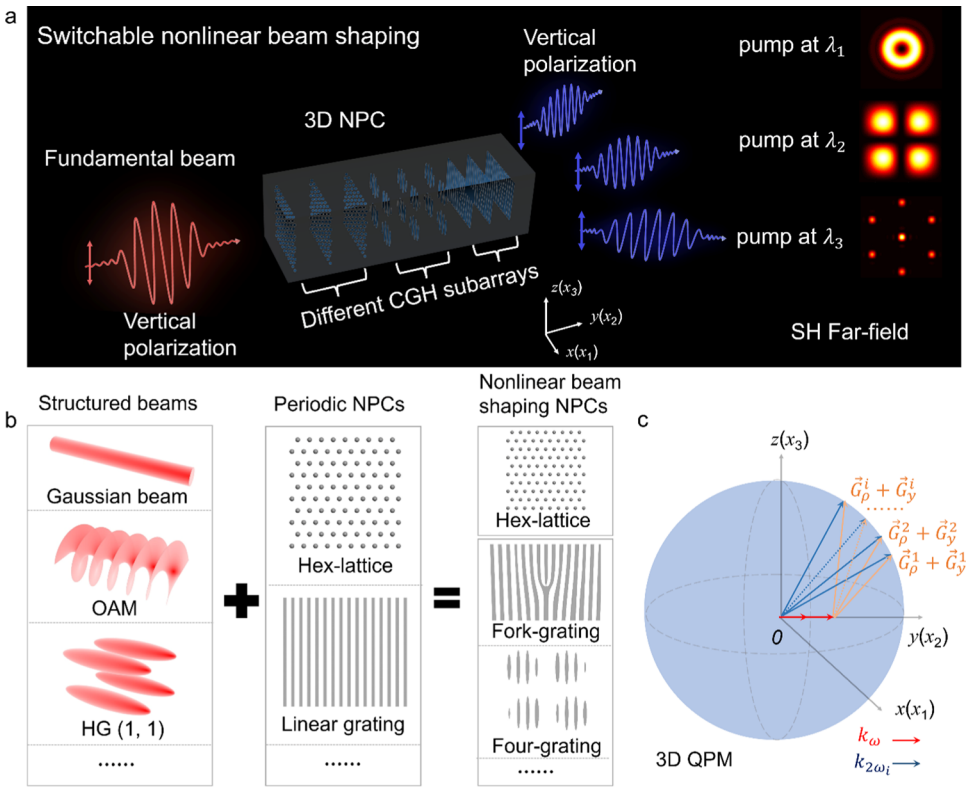

Figure 1. Design principle of 3D NPCs. (a) Schematic representation of the spatial modulation of $\chi^{(2)}$ nonlinearity in 3D NPCs. Each QPM structure provides the needed reciprocal vector to compensate for momentum mismatch in the SH generation process. Here, the ±1st orders show the enhanced SH patterns. The crystal's physical axes (x_1, x_2, x_3) are overlapped with the lab's coordinate systems (x, y, z). (b) Schematic diagram of the combination of structured beams and periodic NPCs. Based on the sequential design idea, different combinations can realize nonlinear beam shaping in different situations. (c) Schematic of QPM in 3D NPCs. NPC, nonlinear photonic crystal; SH, second harmonic; QPM, quasi-phase-matching; 3D, three-dimensional.

nonlinear wave in space. In addition, this technique also breaks through the limitation of QPM materials to achieve efficient deep-ultraviolet SH generation in quartz.[39] Periodic or aperiodic 3D NPCs enable us to break the trade-off in 2D NPC, and have been used to directly generate efficient second-harmonic (SH) structured beams, and realize wavelength-multiplexed SH holography to rebuild a series of intensity patterns.[40−42] However, the coding of multiple complex amplitude beams and switchable reconstruction put forward new demands on 3D NPC, and it is still difficult for the previous schemes to control the complex amplitude of the second harmonic in the wavefront modulation dimension, dynamic switching, and complete QPM at the same time.

In this study, we use the femtosecond laser writing technique to fabricate a 3D NPC that contains sequential $\chi^{(2)}$ nonlinearity modulated arrays for efficient production of switchable SH structured beams. The structure design is based on the complex amplitude CGH[43] and nonlinear Bragg diffraction[44] (a longitudinal reciprocal vector to compensate for the phase mismatching, as a complete 3D QPM). The CGH encodes the SH structured beams into 3D nonlinearity modulation arrays, while the nonlinear Bragg diffraction identifies the desired SH waves *via* the QPM scheme. By sequentially fabricating hexagonal lattice array, four-grating array, and fork-grating array, we demonstrate the switchable conversion of a fundamental Gaussian beam into different SH beams with a conversion efficiency of up to 5.3×10^{-5}. Such nonlinear beam multiplexing will facilitate the development of classical and quantum structured light sources.

RESULTS AND DISCUSSION

Design of the 3D NPCs for Nonlinear Beam Shaping.

Figure 1a shows a schematic diagram of switchable nonlinear beam shaping by fabricating $\chi^{(2)}$ nonlinearity modulation arrays in 3D NPCs. Different CGH subarrays are incorporated into a single $LiNbO_3$ crystal by the femtosecond laser writing technique along the propagation direction, *i.e.*, the y-axis.[45] The CGH subarrays of the 3D NPCs can be expressed as[43,46,47]

$$f(x, y, z) = \sum_i T\{\cos[\vec{G}_\rho^i \rho^i - \arg(E_{2\omega}^i)] - \cos[\sin^{-1}\mathrm{amp}(E_{2\omega}^i)]\} \times T[\cos(\vec{G}_y^i y)] \quad (1)$$

where function T refers to

$$T(s) = \begin{cases} 1, & s \geq 0 \\ 0, & s < 0 \end{cases} \quad (2)$$

In eq 1, $E_{2\omega}^i$ is an i-th designed SH field with its amplitude and phase denoted by " amp" and "arg" functions; ρ^i is the radial coordinate in the x−z plane; $\vec{G}_\rho^i$ is a reciprocal vector along the direction of ρ^i, which is also known as the carrier frequency and affects the diffracted angle of $E_{2\omega}^i$; $\vec{G}_y^i$ is the reciprocal vector along the y-axis to compensate longitudinal phase mismatch; and the summation of "$\sum_i$" refers to the whole modulated process. The Fourier transform of eq 1 is given by

https://doi.org/10.1021/acsphotonics.2c01562
ACS Photonics 2023, 10, 456−463

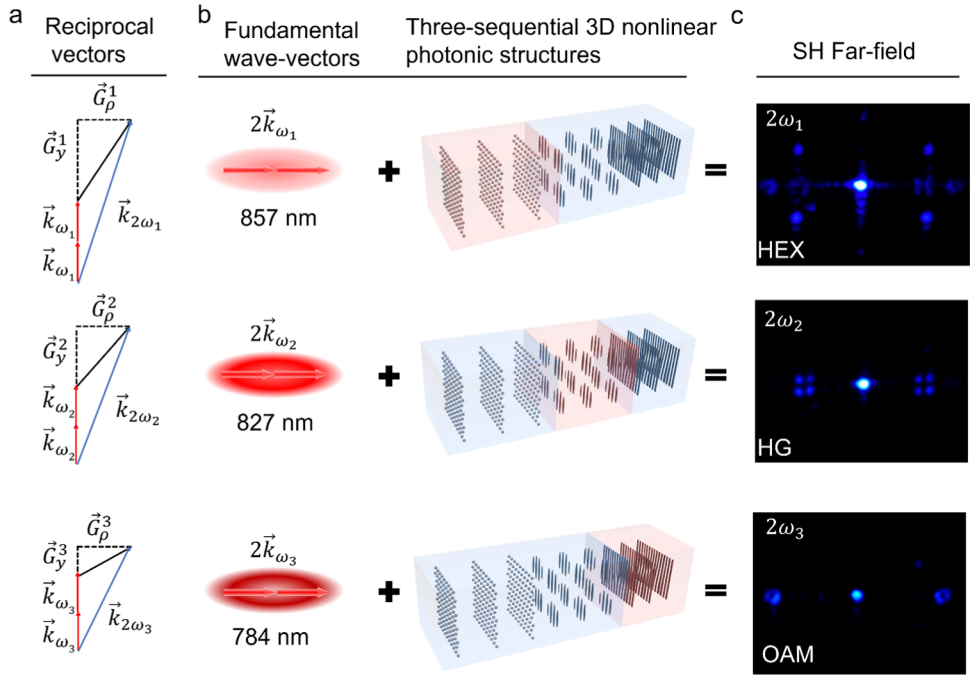

Figure 2. Switchable reconstruction of different SH structured beams. (a) Schematic of the QPM configurations for reconstructing multiple SH structured beams with different wavelengths. (b) Schematic of three-sequential 3D NPCs with different QPM structures. The red region is the action region of fundamental beams with different wavelengths. In our experiment, the intervals in the y-direction for the hexagonal lattice array, four-grating array, and fork-grating array are 3.5, 3, and 2.5 μm, respectively; (c) SH structured beams emitted from different action regions in the three-sequential 3D NPCs at input wavelengths of 857, 827, and 784 nm, respectively.

$$f(x, y, z) = \sum_{i} \sum_{m,n} c^{i}_{m,n} \sin[m \times \sin^{-1} \mathrm{amp}(E^{i}_{2\omega})] e^{i(m\vec{G}^{i}_{\rho}\rho + n\vec{G}^{i}_{y}y)} e^{-im \arg(E^{i}_{2\omega})} \quad (3)$$

where m and n are the order of the reciprocal vectors along ρ^i and y-axis, respectively, and $c_{m,n}$ is the corresponding Fourier coefficient. Clearly, when only considering $m = n = 1$, eq 3 reduces to

$$f(x, y, z) = \sum_{i} c^{i}_{1,1} E^{i}_{2\omega} e^{i(\vec{G}^{i}_{\rho}\rho + \vec{G}^{i}_{y}y)} \quad (4)$$

which recovers the designed SH fields.

The fabrication method can be found in more detail in a previous work.[36] Figure 1b shows that this design method has great flexibility. Periodic photonic crystal structures coded with different structured beams can be combined to abundantly generate and control the output SH pattern. As an experimental demonstration, we designed and fabricated 3D NPCs including hexagonal lattice array, four-grating array, and fork-gratings array. The demonstration here shows the possibilities of our design to achieve popular structured beams, such as HG and LG modes. The hexagonal lattice array with a lattice length of a can be seen as a superposition of plane SH waves with three carrier frequencies $\vec{G}^{i}_{\rho}$ along different directions[48] (Figure S2, Supporting information). The carrier frequencies can be expressed as $\vec{G}^{i}_{\rho} = \frac{4\pi}{\sqrt{3}a}\hat{z}$, $\frac{2\pi}{a}\hat{x} + \frac{2\pi}{\sqrt{3}a}\hat{z}$, $\frac{2\pi}{a}\hat{x} - \frac{2\pi}{\sqrt{3}a}\hat{z}$, respectively. The four-grating and fork-grating can be formed by setting $E^{i}_{2\omega} = \frac{8xz}{w_0^2}\exp\left(-\frac{x^2}{w_0^2}\right)\exp\left(-\frac{z^2}{w_0^2}\right)$ and $E^{i}_{2\omega} = e^{il\varphi}$, respectively, with a carrier frequency of $\vec{G}^{i}_{\rho} = \frac{2\pi}{a}\hat{x}$. It is worth noting that for designing a practical structure, one should consider the QPM condition as well as the nonlinear diffraction angles to obtain the carrier frequencies. The w_0 is the beam waist. The lattice lengths of those structures are different, resulting in different lengths of $\vec{G}^{i}_{\rho}$. Figure 1c shows the switchable reconstruction process through the QPM condition, which can be expressed as

$$\vec{k}_{2\omega} - 2\vec{k}_{\omega} - \vec{G}^{i}_{\rho} - \vec{G}^{i}_{y} = 0 \quad (5)$$

where k_ω and $k_{2\omega}$ are wavevectors of the fundamental beam and the diffracted SH beam, respectively. Although the fundamental beam interacts with all of the 3D NPCs, the generated SH field can only be interfered constructively in a subarray that satisfies eq 5. By tuning the value of $\vec{G}^{i}_{y}$, one can flexibly control the QPM wavelength of $E^{i}_{2\omega}$ to selectively enhance the designed SH structured beam. Here, the conjugate field of $E^{i}_{2\omega}$ also satisfies the QPM condition of eq 5 so that it will be built up simultaneously.

Switchable Reconstruction of Different SH Structured Beams. Figure 2 shows the reconstruction of coded SH beams using different fundamental frequencies *via* nonlinear Bragg diffractions. Optical and SH microscopy images of the three-sequential 3D nonlinear photonics structures are shown in Figure S3 (Supporting information). Three subarrays in the 3D NPC were fabricated along the y-axis, including a hexagonal lattice array, four-grating array, and fork-grating (carrying a topological charge of $l = 1$) in sequence. They have dimensions of 40 μm (x) × 45 μm (z), 32 μm (x) × 32 μm (z), and 45 μm (x) × 40 μm (z) in the x−z plane, and 15 periods along the y-axis with intervals of 3.5, 3, and 2.5 μm, respectively. The carrier frequency of each subarray is

https://doi.org/10.1021/acsphotonics.2c01562
ACS Photonics 2023, 10, 456−463

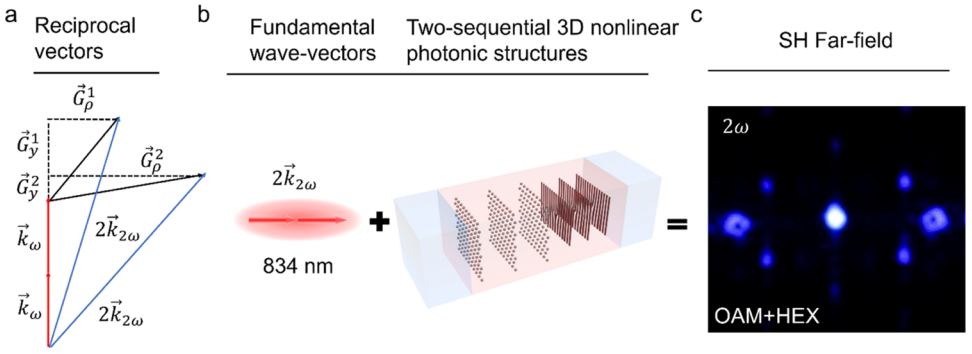

Figure 3. Simultaneous reconstruction of multiple SH structured beams. (a) Schematic of the QPM configurations for reconstructing multiple SH structured beams with a single wavelength; (b) Schematic of two-sequential 3D NPCs with different QPM structures. The red region is the action region of the fundamental beam. In our experiment, the intervals in the *y*-direction for the fork-grating and hexagonal lattices are 3.2 μm. (c) SH structured beams emitted from different action regions in the two-sequential 3D NPCs at an input wavelength of 834 nm.

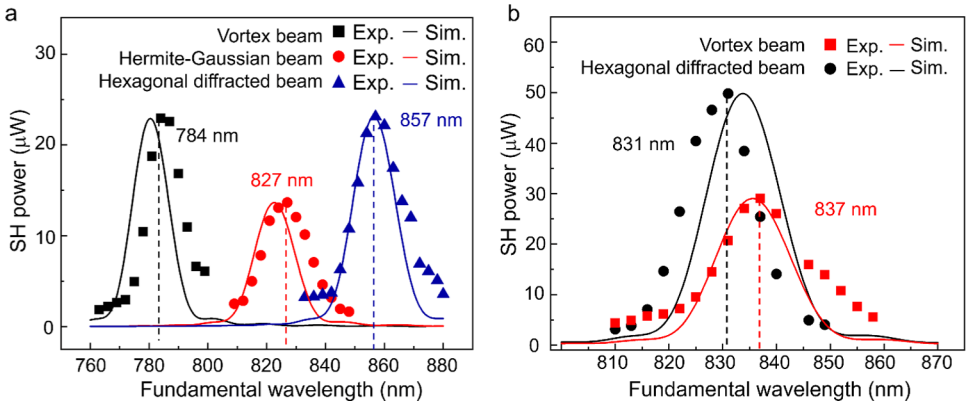

Figure 4. Dependence of the output power of the first diffraction order on the fundamental beam length at a pump power of 1.5 W. (a) The matching wavelengths of the three structured beams are different. (b) The matching wavelengths of the two structured beams are basically the same. The simulated curves agree well with the experimental results.

$\vec{G}_\rho^1 = \frac{\pi}{\sqrt{3}}\hat{z}$, $\frac{\pi}{2}\hat{x} + \frac{\pi}{2\sqrt{3}}\hat{z}$, $\frac{\pi}{2}\hat{x} - \frac{\pi}{2\sqrt{3}}\hat{z}$, $\vec{G}_\rho^2 = \frac{10\pi}{21}\hat{x}$, and $\vec{G}_\rho^3 = \frac{2\pi}{3}\hat{x}$.

As shown in Figure 2b, the fundamental beam with different wavelengths propagates along the *y*-axis to pick out constructively interfering structures through the QPM conditions presented in Figure 2a. Different carrier frequencies and periods lead to diverse $\vec{G}_\rho^i$ and $\vec{G}_y^i$ so that one can control the QPM condition of eq 5*via* wavelengths of the fundamental beam. Figure 2c shows the corresponding far-field SH patterns. When the input wavelength is 857 nm, diffracted SH beams forming six symmetric points in the far field indicate that the SH enhancement mainly comes from the interaction between the fundamental beam and the hexagonal lattice array. Switching the wavelength to 827 nm, the far-field SH pattern turns into HG(1, 1) beams. Further decreasing the wavelength to 784 nm, the buildup of the SH field mainly occurs in the fork-grating array for efficient generation of SH vortex beams. Therefore, the output SH patterns can be changed by tuning the wavelength of the fundamental wave, enabling switching output of nonlinear structured beams. The images in Figure 2c show some visible crosstalk among these far-field SH patterns. The reason is that the hexagonal diffracted SH beam has six light spots, so the average intensity of each point is weak, which results in low contrast. In addition, the focal distortion and elongation caused by refractive index mismatch will affect the laser writing quality, resulting in different brightnesses of the diffracted points. In addition, the zeroth-order SH beam is brighter than high-order diffraction beams because of the larger interaction volume in a collinear SH generation process and the phase mismatch caused by the wide spectrum of the laser. This problem can be effectively solved by increasing the number of cycles of the array and replacing the fundamental beam source with a narrower bandwidth.

Simultaneous Reconstruction of Multiple SH Structured Beams. To further demonstrate the flexibility of SH beam shaping, another 3D NPC is designed to modulate two kinds of nonlinear structured beams with a single fundamental wavelength. Optical and SH microscopy images of the two-sequential 3D nonlinear photonics structures are shown in Figure S4 (Supporting information). This can be achieved by adjusting $\vec{G}_\rho^i$ and $\vec{G}_y^i$ simultaneously so that sequential structures work at the same QPM wavelengths. In the experiment, we design and fabricate two-sequential structures including fork-grating array and hexagonal lattice array. The former has a carrier frequency of $\vec{G}_\rho^1 = \frac{2\pi}{3}\hat{x}$ and a period of 3.2 μm, while the latter has a carrier frequency of $\vec{G}_\rho^2 = \frac{\pi}{\sqrt{3}}\hat{z}$, $\frac{\pi}{2}\hat{x} + \frac{\pi}{2\sqrt{3}}\hat{z}$, $\frac{\pi}{2}\hat{x} - \frac{\pi}{2\sqrt{3}}\hat{z}$ and a period of 3.2 μm, as shown in Figure 3b. Under pump wavelengths of 834 nm, simultaneous nonlinear Bragg diffractions are realized to reconstruct two different beams (Figure 3a). Figure 3c depicts SH patterns emitted from the 3D NPCs, which clearly identify those two kinds of SH beams comprising vortex beams and

https://doi.org/10.1021/acsphotonics.2c01562
ACS Photonics 2023, 10, 456−463

hexagonally diffracted beams that are constructively interfered at the same time. It is further verified that the principle of structure design is that $\vec{G}_{\rho}^{i}$ is mainly used to affect the diffracted angle. Therefore, this method provides a simple way to shape multiple nonlinear beams with controllable amplitude and phase in space.

Conversion Efficiencies for Different SH Structured Beams. The effects of input wavelengths on output powers of different nonlinear beams have been shown in Figure 4. The input power is set to 1.5 W for all of the measurements. For the first 3D NPC (Figure 2), the actual QPM wavelengths can be seen from the peak of the curve in Figure 4a. They are 784 nm for the fork-grating array, 827 nm for the four-grating array, and 857 nm for the hexagonal lattice array, which agree well with the theoretical values of 780, 823, and 856 nm, respectively. Figure 4b shows two nearly overlapping QPM peaks corresponding to the two subarrays in the second 3D NPC. Hence, the SH patterns of the vortex beam and hexagonal diffracted beam are simultaneously enhanced in Figure 3c, distinguishing them from those in Figure 2c. The calculated QPM wavelengths for both subarrays are approximately 834 nm, while the actual QPM wavelengths for the fork-grating array and hexagonal lattice array are 831 and 837 nm, respectively. The emission angles of SH beams are shown in Supporting Information Figure S6 and Table S1. The deviation between the measured and calculated values comes from the laser erasing process. First, the noncrystallization caused by laser exposure changes the refractive index, which was not considered in the calculation process. Second, the aberration caused by refractive index mismatch will affect the uniformity of the fabricated subarrays.[34] When the input fundamental power is 1.5 W, the total conversion efficiencies were 1.3×10^{-5} for three-sequential 3D NPC structure and 5.3×10^{-5} for two-sequential 3D NPC structure, respectively. For sequential NPCs with the ability of multiwavelength-controlled different SH beams, the total conversion efficiency is defined as the average of the conversion efficiency of the sequential 3D NPC structure that generates second-harmonic structured beams under different QPM wavelengths. While, for sequential NPCs with the ability of single-wavelength-modulated multiple SH beams, the total conversion efficiency is defined as the sum of the conversion efficiency mentioned above. The normalized conversion efficiencies for the two 3D NPC structures were 0.52×10^{-10} W^{-1} and 2.12×10^{-10} W^{-1}, respectively. The quantified comparison of the conversion efficiency of different structure light generated by the sequential NPCs and a single NPC are shown in Supporting information Tables S2 and S3. It can be seen that sequential structures provide additional modulation freedoms and also increase a larger propagation loss for the fundamental and second-harmonic waves, resulting in a smaller conversion efficiency compared to the single NPC. To the best of our knowledge, this is the first time to simultaneously modulate multiple nonlinear beams with such considerable conversion efficiencies. In addition, the frequency conversion efficiency is related to the effective length, effective area, duty cycle, modulation type, and so on. For example, these CGH arrays were designed according to the interference between the target beam and the reference beam. For the fork-grating and hexagonal lattice, the corresponding target beam has a uniform amplitude while the target beam of the four-grating has an HG-mode coded amplitude distribution. The amplitude modulation in the nonlinear 3D structure will cause additional losses for the QPM SHG, resulting in a smaller conversion efficiency for the nonlinear Hermite−Gaussian beam.

CONCLUSIONS

We fabricated sequential 3D nonlinear photonic structures using the femtosecond laser writing technique in $LiNbO_3$ and demonstrated switchable conversion of a fundamental Gaussian beam into various SH beams including the hexagonal diffracted beam, the Hermite−Gaussian beam, and the vortex beam. Due to the flexibility of structure design and fabrication techniques, multiwavelength-controlled SH beams and single-wavelength-modulated multiple SH beams have been realized. The nonlinear conversion efficiency is not high although the QPM technique was utilized, which hampers the practical applications of 3D NPCs. Furthermore, on the basis of optimizing the process and reducing the loss, further increasing the length of the array can improve the conversion efficiency and the number of SH beams. Therefore, the 3D NPC provides a simple but efficient way to dynamically control nonlinear beams, which has potential applications in structured beam generation, nonlinear optical encryption, and nonlinear quantum sources.

EXPERIMENT SECTION/METHODS

Fabrication of the 3D NPCs. The femtosecond laser source is a mode-locked Ti:sapphire collocated with a regenerative amplifier (Legend Elite-1K-HE Coherent). The central wavelength is 800 nm, the pulse duration is 104 fs, and the repetition rate is 1 kHz. The laser power is modulated with a half-wave plate and a Glan laser beam splitter. After expansion, the laser is focused by an object lens (50×, NA = 0.8, Olympus) into the $LiNbO_3$ crystal (5% MgO-doped), which is mounted on a piezoelectric platform (E545, from Physik Instrumente GmbH & Co. KG, Germany) with nanometer resolution and a 200 μm × 200 μm × 200 μm moving range. The size of the focal spot inside the crystal is approximately 1.5 μm in X and Y directions and 3 μm in Z direction, which decides the laser writing resolution. To fabricate the fork-grating domains, the laser energy is 180 nJ and the scanning speed is 50 μm s^{-1}. To fabricate the four-grating domains, the laser writing energies are 110 and 150 nJ for the top and bottom layers along the z-axis, respectively. The scanning speed is 50 μm s^{-1}. To fabricate hexagonal lattice domains, the spacing between the 10 layers is 3.5 μm. The writing laser energies are 85, 100, 100, 100, 110, 125, 135, 150, 170, and 170 nJ from top to bottom for 10 layers along the z-axis with the corresponding exposure times of 130, 130, 130, 140, 200, 220, 240, 260, 280, and 300 ms, respectively. In this experiment, these losses were measured to be ∼3.6% for two-sequential 3D NPC structure and ∼5.8% for three-sequential 3D NPC structure.

Nonlinear Beam Shaping Experiment. The fundamental beam outputs from a Ti:sapphire femtosecond laser (Chameleon, Coherent) with a 75 fs pulse duration at 80 MHz repetition. The wavelength is tunable between 690 nm to 1050 nm. The input beam is focused by a lens (f = 100 mm) and incident into the $LiNbO_3$ crystal. The diameter of the beam waist at the focal point is approximately 40 μm and the pump intensity is 1.19×10^3 W mm^{-2}. The crystal's physical axes (x_1, x_2, x_3) are overlapped with the lab's coordinate systems (x, y, z), and the fundamental beam polarizes along the z-axis to utilize the maximal nonlinear coefficient d_{33} in the 3D

https://doi.org/10.1021/acsphotonics.2c01562
ACS Photonics 2023, 10, 456−463

$LiNbO_3$ NPCs. The output far-field SH patterns are projected on a white screen and then recorded by a camera. The powers of SH are measured by a power meter. For the Hermite−Gaussian beam and vortex beam, the powers of the ±1st nonlinear diffraction orders were measured. For the hexagonal diffracted beam, the powers of six bright spots were measured. The measurements of topological charges are shown in Figure S5 (Supporting information).

■ ASSOCIATED CONTENT

Supporting Information

The Supporting Information is available free of charge at https://pubs.acs.org/doi/10.1021/acsphotonics.2c01562.

Real space distribution of the hexagonal lattice, optical microscopy and Cerenkov second-harmonic microscopy for the nonlinear photonics structures, measured results of topological charges, measured and calculated emission angles, and quantified comparison of the conversion efficiency for sequential 3D NPC and single NPC (PDF)

■ AUTHOR INFORMATION

Corresponding Authors

Yong Zhang − *National Laboratory of Solid State Microstructures, College of Engineering and Applied Sciences, School of Physics, and Collaborative Innovation Center of Advanced Microstructures, Nanjing University, Nanjing 210093, China;* orcid.org/0000-0003-1158-2248; Email: zhangyong@nju.edu.cn

Dong Wu − *Hefei National Laboratory for Physical Sciences at the Microscale and CAS Key Laboratory of Mechanical Behavior and Design of Materials, Department of Precision Machinery and Precision Instrumentation, University of Science and Technology of China, Hefei 230026, China;* orcid.org/0000-0003-0623-1515; Email: dongwu@ustc.edu.cn

Authors

Chaowei Wang − *Hefei National Laboratory for Physical Sciences at the Microscale and CAS Key Laboratory of Mechanical Behavior and Design of Materials, Department of Precision Machinery and Precision Instrumentation, University of Science and Technology of China, Hefei 230026, China*

Pengcheng Chen − *National Laboratory of Solid State Microstructures, College of Engineering and Applied Sciences, School of Physics, and Collaborative Innovation Center of Advanced Microstructures, Nanjing University, Nanjing 210093, China*

Dunzhao Wei − *State Key Laboratory of Optoelectronic Materials and Technologies, School of Physics, Sun Yat-Sen University, Guangzhou 510275, China*

Leran Zhang − *Hefei National Laboratory for Physical Sciences at the Microscale and CAS Key Laboratory of Mechanical Behavior and Design of Materials, Department of Precision Machinery and Precision Instrumentation, University of Science and Technology of China, Hefei 230026, China*

Zihang Zhang − *Hefei National Laboratory for Physical Sciences at the Microscale and CAS Key Laboratory of Mechanical Behavior and Design of Materials, Department of Precision Machinery and Precision Instrumentation, University of Science and Technology of China, Hefei 230026, China*

Liqun Xu − *Hefei National Laboratory for Physical Sciences at the Microscale and CAS Key Laboratory of Mechanical Behavior and Design of Materials, Department of Precision Machinery and Precision Instrumentation, University of Science and Technology of China, Hefei 230026, China*

Yanlei Hu − *Hefei National Laboratory for Physical Sciences at the Microscale and CAS Key Laboratory of Mechanical Behavior and Design of Materials, Department of Precision Machinery and Precision Instrumentation, University of Science and Technology of China, Hefei 230026, China;* orcid.org/0000-0003-1964-0043

Jiawen Li − *Hefei National Laboratory for Physical Sciences at the Microscale and CAS Key Laboratory of Mechanical Behavior and Design of Materials, Department of Precision Machinery and Precision Instrumentation, University of Science and Technology of China, Hefei 230026, China;* orcid.org/0000-0003-3950-6212

Min Xiao − *National Laboratory of Solid State Microstructures, College of Engineering and Applied Sciences, School of Physics, and Collaborative Innovation Center of Advanced Microstructures, Nanjing University, Nanjing 210093, China; Department of Physics, University of Arkansas, Fayetteville, Arkansas 72701, United States*

Jiaru Chu − *Hefei National Laboratory for Physical Sciences at the Microscale and CAS Key Laboratory of Mechanical Behavior and Design of Materials, Department of Precision Machinery and Precision Instrumentation, University of Science and Technology of China, Hefei 230026, China;* orcid.org/0000-0001-6472-8103

Complete contact information is available at: https://pubs.acs.org/10.1021/acsphotonics.2c01562

Author Contributions

⊥C.W., P.C., and D.W. contributed equally to this paper. The manuscript was written through contributions of all authors. All authors have given approval to the final version of the manuscript.

Funding

This work was supported by the National Natural Science Foundation of China (nos. 61927814, 62005262, 11904424, 91950206), the China Postdoctoral Science Foundation (2021T140649), the USTC Research Funds of the Double First-Class Initiative (YD2340002009), CAS Youth Interdisciplinary Team (JCTD-2021-20), Guangdong Natural Science Funds for Distinguished Young Scholars (2022B1515020067), Guangzhou Science and Technology Plan Foundation and Application Foundation Research Project (202201011270), and the Strategic Priority Research Program of the Chinese Academy of Sciences XDA16021200.

Notes

The authors declare no competing financial interest.

■ ACKNOWLEDGMENTS

The authors acknowledge the Experimental Center of Engineering and Material Sciences at USTC for the fabrication and measuring of samples. This work was partly carried out at the USTC Center for Micro and Nanoscale Research and Fabrication.

REFERENCES

(1) Forbes, A.; Oliveira, M.; Dennis, M. Structured light. *Nat. Photonics* **2021**, *15*, 253−262.
(2) Forbes, A. Structured light from lasers. *Laser Photonics Rev.* **2019**, *13*, No. 1900140.
(3) Deng, Z.; Jin, M.; Ye, X.; Wang, S.; Shi, T.; Deng, J.; Mao, N.; Cao, Y.; Guan, B.; Alu, A.; Li, G.; Li, X. Full-Color Complex-Amplitude Vectorial Holograms Based on Multi-Freedom Metasurfaces. *Adv. Funct. Mater.* **2020**, *30*, No. 1910610.
(4) Deng, Z.; Tu, Q.; Wang, Y.; Wang, Z.; Shi, T.; Feng, Z.; Qiao, X.; Wang, G.; Xiao, S.; Li, X. Vectorial Compound Metapixels for Arbitrary Nonorthogonal Polarization Steganography. *Adv. Mater.* **2021**, *33*, No. 2103472.
(5) Wei, B.; Hu, W.; Ming, Y.; Xu, F.; Rubin, S.; Wang, J.; Chigrinov, V.; Lu, Y. Generating switchable and reconfigurable optical vortices via photopatterning of liquid crystals. *Adv. Mater.* **2014**, *26*, 1590−1595.
(6) Ge, S.-J.; Ji, W.; Cui, G.; Wei, B.; Hu, W.; Lu, Y. Fast switchable optical vortex generator based on blue phase liquid crystal fork grating. *Opt. Mater. Express* **2014**, *4*, 2535−2541.
(7) Avayu, O.; Eisenbach, O.; Ditcovski, R.; Ellenbogen, T. Optical metasurfaces for polarization-controlled beam shaping. *Opt. Lett.* **2014**, *39*, 3892−3895.
(8) Holsteen, A. L.; Cihan, A.; Brongersma, M. Temporal color mixing and dynamic beam shaping with silicon metasurfaces. *Science* **2019**, *365*, 257−260.
(9) Huang, C.; Zhang, C.; Xiao, S.; Wang, Y.; Fan, Y.; Liu, Y.; Zhang, N.; Qu, G.; Ji, H.; Han, J.; Ge, L.; Kivshar, Y.; Song, Q. Ultrafast control of vortex microlasers. *Science* **2020**, *367*, 1018−1021.
(10) Azzam, S. I.; Chaudhuri, K.; Lagutchev, A.; Jacob, Z.; Kim, Y.; Shalaev, V.; Boltasseva, A.; Kildishev, A. Single and Multi-Mode Directional Lasing from Arrays of Dielectric Nanoresonators. *Laser Photonics Rev.* **2021**, *15*, No. 2000411.
(11) Berger, V. Nonlinear photonic crystals. *Phys. Rev. Lett.* **1998**, *81*, 4136.
(12) Broderick, N. G. R.; Ross, G.; Offerhaus, H.; Richardson, D.; Hanna, D. Hexagonally poled lithium niobate: a two-dimensional nonlinear photonic crystal. *Phys. Rev. Lett.* **2000**, *84*, 4345.
(13) Fang, X.; Yang, H.; Yao, W.; Wang, T.; Zhang, Y.; Gu, M.; Xiao, M. High-dimensional orbital angular momentum multiplexing nonlinear holography. *Adv. Photonics* **2021**, *3*, No. 015001.
(14) Hong, X.-H.; Yang, B.; Zhang, C.; Qin, Y.; Zhu, Y. Nonlinear volume holography for wave-front engineering. *Phys. Rev. Lett.* **2014**, *113*, No. 163902.
(15) Segal, N.; Keren-Zur, S.; Hendler, N.; Ellenbogen, T. Controlling light with metamaterial-based nonlinear photonic crystals. *Nat. Photonics* **2015**, *9*, 180−184.
(16) Almeida, E.; Bitton, O.; Prior, Y. Nonlinear metamaterials for holography. *Nat. Commun.* **2016**, *7*, No. 12533.
(17) Frese, D.; Wei, Q.; Wang, Y.; Cinchetti, M.; Huang, L.; Zentgraf, T. Nonlinear bicolor holography using plasmonic metasurfaces. *ACS Photonics* **2021**, *8*, 1013−1019.
(18) Ye, W.; Zeuner, F.; Li, X.; Reineke, B.; He, S.; Qiu, C.; Liu, J.; Wang, Y.; Zhang, S.; Zentgraf, T. Spin and wavelength multiplexed nonlinear metasurface holography. *Nat. Commun.* **2016**, *7*, No. 11930.
(19) Li, J.; Hu, G.; Shi, L.; He, N.; Li, D.; Shang, Q.; Zhang, Q.; Fu, H.; Zhou, L.; Xiong, W.; Guan, J.; Wang, J.; He, S.; Chen, L. Full-color enhanced second harmonic generation using rainbow trapping in ultrathin hyperbolic metamaterials. *Nat. Commun.* **2021**, *12*, No. 6425.
(20) Keren-Zur, S.; Avayu, O.; Michaeli, L.; Ellenbogen, T. Nonlinear Beam Shaping with Plasmonic Metasurfaces. *ACS Photonics* **2016**, *3*, 117−123.
(21) Armstrong, J. A.; Bloembergen, N.; Ducuing, J.; Pershan, P. Interactions between light waves in a nonlinear dielectric. *Phys. Rev.* **1962**, *127*, 1918.
(22) Zhu, S.-n.; Zhu, Y.; Ming, N. Quasi-phase-matched third-harmonic generation in a quasi-periodic optical superlattice. *Science* **1997**, *278*, 843−846.
(23) Liu, H.; Li, J.; Zhao, X.; Zheng, Y.; Chen, X. Nonlinear Raman-Nath second harmonic generation with structured fundamental wave. *Opt. Express* **2016**, *24*, 15666−15671.
(24) Wang, X.; Cao, J.; Zhao, X.; Zheng, Y.; Ren, H.; Deng, X.; Chen, X. Sum-frequency nonlinear Cherenkov radiation generated on the boundary of bulk medium crystal. *Opt. Express* **2015**, *23*, 31838−31843.
(25) Freund, I. Nonlinear diffraction. *Phys. Rev. Lett.* **1968**, *21*, 1404.
(26) Arie, A.; Habshoosh, N.; Bahabad, A. Quasi phase matching in two-dimensional nonlinear photonic crystals. *Opt. Quantum Electron.* **2007**, *39*, 361−375.
(27) Li, G.; Zhang, S.; Zentgraf, T. Nonlinear photonic metasurfaces. *Nat. Rev. Mater.* **2017**, *2*, No. 17010.
(28) Neira, A. D.; Olivier, N.; Nasir, M.; Dickson, W.; Wurtz, G.; Zayats, A. Eliminating material constraints for nonlinearity with plasmonic metamaterials. *Nat. Commun.* **2015**, *6*, No. 7757.
(29) Lu, C.; Hu, X.; Shi, K.; Hu, Q.; Zhu, R.; Yang, H.; Gong, Q. An actively ultrafast tunable giant slow-light effect in ultrathin nonlinear metasurfaces. *Light: Sci. Appl.* **2015**, *4*, e302.
(30) Liu, H.; Guo, C.; Vampa, G.; Zhang, J.; Sarmiento, T.; Xiao, M.; Bucksbaum, P.; Vuckovic, J.; Fan, S.; Reis, D. Enhanced high-harmonic generation from an all-dielectric metasurface. *Nat. Phys.* **2018**, *14*, 1006−1010.
(31) Ellenbogen, T.; Voloch-Bloch, N.; Ganany-Padowicz, A.; Arie, A. Nonlinear generation and manipulation of Airy beams. *Nat. Photonics* **2009**, *3*, 395−398.
(32) Trajtenberg-Mills, S.; Juwiler, I.; Arie, A. Generation of second-harmonic beams with switchable curved trajectories. *Optica* **2017**, *4*, 153−156.
(33) Dolev, I.; Ellenbogen, T.; Arie, A. Switching the acceleration direction of Airy beams by a nonlinear optical process. *Opt. Lett.* **2010**, *35*, 1581−1583.
(34) Shapira, A.; Juwiler, I.; Arie, A. Tunable nonlinear beam shaping by non-collinear interactions. *Laser Photonics Rev.* **2013**, *7*, L25−L29.
(35) Xu, T.; Switkowski, K.; Chen, X.; Liu, S.; Koynov, K.; Yu, H.; Zhang, H.; Wang, J.; Sheng, Y.; Krolikowski, W. Three-dimensional nonlinear photonic crystal in ferroelectric barium calcium titanate. *Nat. Photonics* **2018**, *12*, 591−595.
(36) Wei, D.; Wang, C.; Wang, H.; Hu, X.; Wei, D.; Fang, X.; Zhang, Y.; Wu, D.; Hu, Y.; Li, J.; Zhu, S.; Xiao, M. Experimental demonstration of a three-dimensional lithium niobate nonlinear photonic crystal. *Nat. Photonics* **2018**, *12*, 596−600.
(37) Liu, S.; Switkowski, K.; Xu, C.; Tian, J.; Wang, B.; Lu, P.; Krolikowski, W.; Sheng, Y. Nonlinear wavefront shaping with optically induced three-dimensional nonlinear photonic crystals. *Nat. Commun.* **2019**, *10*, No. 3208.
(38) Imbrock, J.; Wesemann, L.; Kroesen, S.; Ayoub, M.; Denz, C. Waveguide-integrated three-dimensional quasi-phase-matching structures. *Optica* **2020**, *7*, 28−34.
(39) Shao, M.; Liang, F.; Yu, H.; Zhang, H. Angular engineering strategy of an additional periodic phase for widely tunable phase-matched deep-ultraviolet second harmonic generation. *Light: Sci. Appl.* **2022**, *11*, No. 31.
(40) Liu, S.; Mazur, L.; Krolikowski, W.; Sheng, Y. Nonlinear volume holography in 3D nonlinear photonic crystals. *Laser Photonics Rev.* **2020**, *14*, No. 2000224.
(41) Wei, D.; Wang, C.; Xu, X.; Wang, H.; Hu, Y.; Chen, P.; Li, J.; Zhu, Y.; Xin, C.; Hu, X.; Zhang, Y.; Wu, D.; Chu, J.; Zhu, S.; Xiao, M. Efficient nonlinear beam shaping in three-dimensional lithium niobate nonlinear photonic crystals. *Nat. Commun.* **2019**, *10*, No. 4193.
(42) Chen, P.; Wang, C.; Wei, D.; Hu, Y.; Xu, X.; Li, J.; Wu, D.; Ma, J.; Ji, S.; Zhang, L.; Xu, L.; Wang, T.; Xu, C.; Chu, J.; Zhu, S.; Xiao, M.; Zhang, Y. Quasi-phase-matching-division multiplexing holography in a three-dimensional nonlinear photonic crystal. *Light: Sci. Appl.* **2021**, *10*, No. 146.
(43) Lee, W.-H. Binary computer-generated holograms. *Appl. Opt.* **1979**, *18*, 3661−3669.

https://doi.org/10.1021/acsphotonics.2c01562
ACS Photonics 2023, 10, 456−463

(44) Zhang, J.; Zhao, X.; Zheng, Y.; Li, H.; Chen, X. Universal modeling of second-order nonlinear frequency conversion in three-dimensional nonlinear photonic crystals. *Opt. Express* **2018**, *26*, 15675−15682.
(45) Li, L.; Kong, W.; Chen, F. Femtosecond laser-inscribed optical waveguides in dielectric crystals: a concise review and recent advances. *Adv. Photonics* **2022**, *4*, No. 024002.
(46) Shapira, A.; Shiloh, R.; Juwiler, I.; Arie, A. Two-dimensional nonlinear beam shaping. *Opt. Lett.* **2012**, *37*, 2136−2138.
(47) Epstein, I.; Lilach, Y.; Arie, A. Shaping plasmonic light beams with near-field plasmonic holograms. *J. Opt. Soc. Am. B* **2014**, *31*, 1642−1647.
(48) Xu, P.; Ji, S.; Zhu, S.; Yu, X.; Sun, J.; Wang, H.; He, J.; Zhu, Y.; Ming, N. Conical Second Harmonic Generation in a Two-Dimensional $\chi^{(2)}$ Photonic Crystal: A Hexagonally Poled LiTaO3 Crystal. *Phys. Rev. Lett.* **2004**, *93*, No. 133904.

https://doi.org/10.1021/acsphotonics.2c01562
ACS Photonics 2023, 10, 456−463